coatings

MDPI

Article

Superlubricity of Titanium Alloy Enabled by MoS_2 Flakes and a-C:H Film

Weipeng Liu [1], Wenchao Wu [2], Muhammad Chhattal [2], Qingkai Zheng [2], Xinchen Gao [2], Kexin Ren [2], Guangqiao Liu [3], Zhongrong Geng [1,*] and Zhenbin Gong [2,*]

[1] School of Mechanical Engineering, Lanzhou Jiaotong University, Lanzhou 730070, China; 17361560709@163.com
[2] State Key Laboratory of Solid Lubrication, Lanzhou Institute of Chemical Physics, Chinese Academy of Sciences, Lanzhou 730000, China; wuwenchao@licp.cas.cn (W.W.); chhattal@outlook.com (M.C.); zhengqingkai@licp.cas.cn (Q.Z.); c18406581419@163.com (X.G.); 17862705505@163.com (K.R.)
[3] Bailie School of Petroleum Engineering, Lanzhou City University, Lanzhou 730070, China; liugq1968@163.com
* Correspondence: gzrong-1977@163.com (Z.G.); gongzhenbin@licp.cas.cn (Z.G.)

Abstract: Titanium alloys are often used in engineering fields including aerospace, cryogenic technologies, and weaponry due to their remarkable qualities. However, several issues including a high coefficient of friction, weak wear resistance, and low hardness hinder their widespread usage. Despite several efforts to enhance their tribology, achieving ultra-low friction on titanium alloy surfaces remains a challenging problem in materials science. Here, we report on the superlubricity of a MoS_2 + a-C:H (Mo-a films) composite film, prepared by magnetron sputtering and spraying to lubricate titanium alloy surfaces. Robust superlubricity was achieved by the Mo-a composite films with a coefficient of friction (COF) below 0.007 in a helium environment. Compared to the reference titanium alloy substrates, the introduction of Mo-a composite film reduced the friction coefficient to roughly 1%, and the a-C:H film reduced wear by three orders of magnitude. High-resolution characterizations indicate that this enhanced tribology can be attributed to the formation of transfer film, which is enriched with nanostructured graphene sheets and MoS_2 nanoscrolls, and is formed due to shear stress-induced structural transformation of a-C:H films and MoS_2 nanosheets. This transfer film transitioned the initial high-resistance steel-to-a-C:H contact to super low-resistance steel-to-transfer film contact, thus achieving superlubricity and a remarkable wear reduction. This work outlines a pathway to solving the poor wear resistance and high friction coefficient problem of titanium alloy surfaces, which can be an important guideline for applications of titanium alloys in mechanical engineering.

Keywords: MoS_2; amorphous carbon film; titanium alloy; superlubricity; friction

Citation: Liu, W.; Wu, W.; Chhattal, M.; Zheng, Q.; Gao, X.; Ren, K.; Liu, G.; Geng, Z.; Gong, Z. Superlubricity of Titanium Alloy Enabled by MoS_2 Flakes and a-C:H Film. *Coatings* **2023**, *13*, 820. https://doi.org/10.3390/coatings13050820

Academic Editor: Ivan A. Pelevin

Received: 23 March 2023
Revised: 11 April 2023
Accepted: 13 April 2023
Published: 23 April 2023

1. Introduction

Friction and wear are the most problematic challenges for mechanical systems, resulting in material loss, environmental pollution, and dramatically limiting the reliability, efficiency, and service life [1]. To answer these tribological challenges, advanced new materials, novel technologies, and novel strategies to control the friction and wear are paramount for the reliable and effective use of modern-day equipment [2–5]. In this pursuit, titanium alloys have been extensively used in aviation, marine, and weapons because of their excellent comprehensive performance, high temperature, high pressure, and corrosion resistance [6]. However, titanium alloys exhibit a high friction coefficient and poor wear resistance because of their high adhesion, low hardness, and low elastic modulus, which limits their engineering applications [7]. To improve the tribological performance of titanium alloys, several surface treatment technologies such as chemical vapor deposition, spraying, and laser processing are widely used [8]. Published research has established that

titanium nitride (TiN), titanium aluminum nitride (TiAlN), titanium carbonitride (TiCN), and diamond-like carbon (DLC) films have good friction and wear properties and are employed on metal surfaces to prolong the service life of sliding parts [9–12]. DLC films have drawn much attention in this quest due to their high hardness, chemical inertness, low friction properties, and low wear [13,14]. For example, Liu et al. deposited DLC films on the surface of a titanium alloy previously implanted with carbon ions by plasma-enhanced chemical vapor deposition (PECVD); for the prepared film, the COF was around 0.1, which was about 1/3 of the reference titanium substrate [15]. In another study, Zhang et al. prepared DLC films with different nest area densities on the Ti–6Al–4V surfaces using magnetron sputtering and laser surface texturing techniques. The results show that DLC films with different dimple area densities affect the tribological properties, with dimple area densities close to 44% having good friction reduction and dimple densities close to 24% having excellent wear resistance [16]. Even though the DLC film had excellent wear resistance, the friction coefficient was still higher than 0.1; to mitigate these problems of DLC films, recently, efforts have been made to fabricate the heterostructures by combining MoS_2 with other two-dimensional materials and DLC coatings [17,18]. Theoretical calculations show that the fabrication of heterostructures offers the possibility of achieving superlubricity because the energy consumption by the friction of the hierarchical structure is an order of magnitude less than that of each component [19]. For example, Zhang et al. achieved superlubricity on the silicon substrate by fabricating MoS_2 and DLC heterostructures, which was attributed to the fact that the fabrication of the heterostructures effectively suppressed the dissipation of energy in the friction process [20]. Zhang et al. prepared MoS_2 and graphite-like heterostructures by magnetron sputtering and PECVD, achieving superlubricity even at high speeds and loads [21]. Sumant et al. realized superlubricity via MoS_2 and nanodiamonds on a Si substrate, where the in situ formation of onion-like carbon nanoscrolls reduced the contact surface and led to incommensurate contact [22]. Sumant et al. obtained a low friction coefficient of 0.018 by graphene + MoS_2 films at the sliding interface in the friction process [23]. Other studies have demonstrated that heterogeneous structures have the potential to reduce friction and wear, providing strong evidence for understanding the superlubricity mechanisms and designing lubricating interfaces [24,25]. However, many studies have shown that the high internal stresses within DLC films make them difficult to deposit directly on titanium alloys and other metal substrates, resulting in films that tend to flake off under experimental conditions [26,27]. The engineering applications with hierarchical structures on the surface of titanium alloys are still challenging [28].

In this study, we fabricated a composite film made of a-C:H film and MoS_2 nanosheets on the surface of titanium alloys using magnetron sputtering and spraying. The tribological behavior of the composite film under different loads was investigated using a reciprocating tribometer. The results show that compared to the reference titanium alloy samples, the Mo-a films reduced friction and wear, achieving a superlubricity state with 0.007, which establishes that Mo-a composite films are useful for lubricating titanium alloy surfaces. Furthermore, we also found that the production of an oriented MoS_2 and graphene-like structure and its structural transformation into a MoS_2 nanoscroll facilitates the achievement of superlubricity. The introduction of the composite films achieved the superlubricity of titanium alloys and provided a strategy for designing superlubricity on metal surfaces.

2. Experimental Methods

2.1. Materials

MoS_2 flakes were purchased from ZhongNuo Advanced Material (Beijing, China) Technology Co., Ltd. Ti targets (>99.99%) were acquired from Sinova New Material (Beijing, China) Technology Co., Ltd.

2.2. The Preparation of a-C:H Film

A high vacuum multi-functional magnetron sputtering ion coating system equipped with argon and methane gas sources was used to deposit composite Ti/TiC/a-C:H films

onto a titanium alloy in an argon/methane atmosphere. Before the deposition of the film on the substrate, the surface of the titanium alloy was rubbed with sandpaper of different grit sizes (400#, 800#, 1000#, 1500#, and 2000#) to remove surface oxides and impurities. The polished titanium alloy substrates and silicon wafers (2×2 cm^2) were then ultrasonically cleaned for 30 min in an ethanol solution. After cleaning, the substrates were mounted on a revolving rack on the vacuum chamber's sample table. To begin the film deposition process, argon gas was introduced into the vacuum chamber at a flow rate of 17 sccm when the chamber pressure reached 1.0×10^{-3} Pa through mechanical and molecular pumps. The substrate was then cleaned for 30 min at a 406 V bias voltage. The overall interlayer film deposition process of the composite film is as follows:

(1) Titanium layer deposition: The titanium layer was deposited for 30 min at a rate of 120 sccm of argon flow, 100 V of bias voltage, and 2 A of sputtering current.
(2) Titanium carbide interlayer deposition: First, the argon flow rate was adjusted to 30 sccm for the deposition of the titanium carbide interlayer, and the methane flow rate was increased from 8 sccm to 30 sccm with a gradient of 2 sccm every 3 min.
(3) a-C:H layer deposition: For the deposition of the a-C:H layer, the sputtering power was turned off, and methane was introduced at the flow rate of 30 sccm, bias voltage 800 V, and was deposited for 120 min.

2.3. The Preparation of MoS_2 + a-C:H Film

For the preparation of the MoS_2 + a-C:H film, 40 mg of MoS_2 powder was added into 5 mL of ethanol (concentration of 8 mg/mL) and ultrasonicated for 30 min. Then, 1 mL of the as-prepared MoS_2 solution was sprayed on the surface of the 2×2 cm^2 a-C:H film. Thus, the Mo-a film was obtained when complete ethanol solvent was evaporated under light-assisted irradiation. For comparative analysis, 1 mL of the MoS_2 dispersion was sprayed on the titanium alloy substrate to fabricate a MoS_2 film.

2.4. Structure Characterizations

The microstructure, surface morphology, and elemental distribution of the as-prepared films were investigated by scanning electron microscopy (Japan Electronics Company, JSM-5601LV, Toyama, Japan). The cross-section of a-C:H film on a Si substrate was observed by field emission scanning electron microscopy (Japan Electronics Company, JSM-6701F, Toyama, Japan) at 5.0 kV. The counterpart ball's wear debris nanostructure was investigated with field emission electron microscopy (FEI company, TF20, Hillsboro, OR, USA). The wear tracks and scars were investigated by Raman spectroscopy at a laser wavelength of 532 nm with a LabRam HR800 spectrometer (HORIBA Jobin Yvon S.A.S, LabRAM HR Evolution, Palaiseau, France). The hardness, elastic modulus, and elastic recovery rate of a-C:H film were measured by the Hit 300 nanoindentation tester. To investigate the anti-wear performance of the Mo-a film, MoS_2 samples, a-C:H samples, and titanium alloy samples under different loads were characterized with a MAX 3D surface profiler (KLA-Tencor, MicroXAM-800, Milpitas, CA, USA) after the friction tests.

2.5. Tribological Testing

In linear reciprocating sliding mode, friction tests were conducted using a ball-on-disk tribometer (Anton Paar, CSM TBR^3, Buchs, Switzerland) with normal loads of 1, 3, 5, 7, 9, and 11 N, and 6 mm diameter steel balls were used as a sliding counterpart. Before each experiment, high-purity helium was introduced, and the experiment was started once the relative humidity fell to 5%. The reciprocating frequency and the amplitude for each test were set to 5 Hz and 5 mm, respectively. All of the friction tests were repeated three times to ensure the stability and repeatability of the test results.

2.6. Nanoindentation Tests

The modulus of elasticity R was calculated using Equation (1), where d_{max} is the maximum displacement at maximum load, and d_{res} is the residual displacement after unloading.

$$R = (d_{max} - d_{res})/d_{max} \times 100\% \quad (1)$$

2.7. Wear Rate Calculation

In addition, the wear rates were calculated according to the Equation (2):

$$W = V/F \times L \quad (2)$$

where W ($mm^3/N^{-1} \cdot m^{-1}$) is the wear rate; V is the wear volume; F is the applied normal load; L is the sliding length.

3. Results and Discussion

3.1. Structural and Composition Analysis

Figure 1a shows the schematic of the ball-on-disk reciprocating friction experiment setup, which was used to study the friction of the Mo-a film and steel counter ball in a helium atmosphere. The mechanical properties of the a-C:H films are displayed in Figure 1b; the elastic modulus, hardness, and elastic recovery of the a-C:H films were 131.8 GPa, 11.3 GPa, and 62%, respectively, which shows that a-C:H films had outstanding mechanical properties. Figure 1c shows the Raman spectrum of the a-C:H film, where the D peak and G peak of the a-C:H film appeared at 1407 and 1539 cm^{-1}, corresponding to the respiratory vibration mode of the aromatic ring and the vibration stretching mode of the sp^2 site pair in the aromatic or alkene chain, respectively [29,30]. The intensity variations in the characteristic peaks of the a-C:H films provide important information for probing the structural changes at the friction interface. The intensity ratio of the D and G peaks (I_D/I_G) of the a-C:H film was 0.58. Figure 1d shows that there was only a weak G peak and no D peak in the Raman spectrum of the Mo-a composite film, which indicates that the a-C:H film was almost completely covered by the MoS_2 film. Moreover, two narrow and sharp peaks near 378 and 404 cm^{-1} were the E^1_{g2} and the A1g signals, corresponding to MoS_2. E^1_{g2} is the signal generated by the reverse vibration of two S atoms in the fundamental plane for one Mo atom, while A_{1g} is caused by the out-of-plane or vertical vibration of the S atom in the opposite direction [31]. The surface morphology of the Mo-a film sample is shown in Figure 1e, with a large amount of MoS_2 sheets distributed on the surface of the a-C:H film. Figure 1f shows the distribution of the C, S, Mo, and O elements in the surface of the a-C:H film. It can be seen that there were a large number of Mo and S elements distributed on the surface of the a-C:H film, which also demonstrates that the a-C:H film surface was entirely covered by MoS_2. Figure 1g shows a cross-sectional image of the a-C:H film. From the cross-section of the film, it can be seen that the multilayer film structure comprised the Ti layer, the TiC interlayer, and the a-C:H layer, with an overall thickness of 2.98 μm with a clear boundary between each layer. The thickness of the bottom Ti layer was approximately 1.16 μm, the middle transition layer TiC was approximately 0.22 μm, and the top a-C:H layer was about 1.60 μm. Figure 1h shows the elemental mapping of the a-C:H film, where it can be seen that the cross-sectional region had a large amount of Ti and C elements.

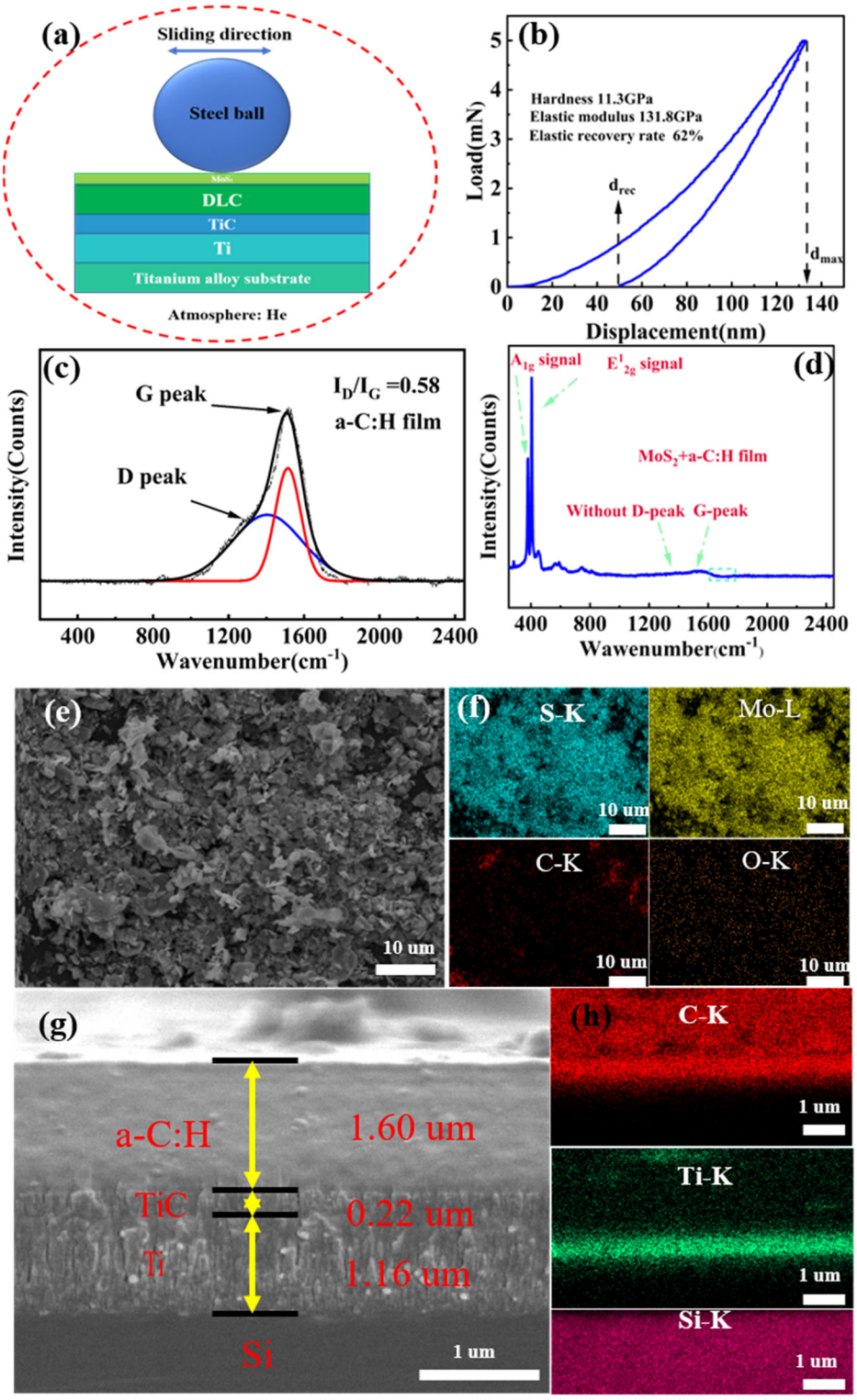

Figure 1. (**a**) Illustration of the composite film material composition and friction test. (**b**) The mechanical properties of the prepared a−C:H film. (**c**) Raman spectrum of the as-deposited a−C:H film. (**d**) Raman spectrum of the as−deposited Mo-a films. (**e**) The surface SEM image of the Mo-a films. (**f**) The local distribution of the Mo, S, C, and O elements on the surface of the Si substrate. (**g**) The cross-sectional SEM image of the a−C:H film. (**h**) The cross-sectional elemental mapping of the a−C:H film.

3.2. Tribological Performance Analysis

The tribological performances of the as-prepared a-C:H film, titanium alloy, MoS_2 coating, and Mo-a film relative to a steel ball sliding under a 5 N load in a helium environment are shown in Figure 2a. It can be seen that the friction coefficient of the steel ball sliding on the reference titanium alloy was 0.371, as shown in the inset of Figure 2a. This COF is very high, possibly due to the evaluation of the wear debris. After spraying the MoS_2 solution onto the titanium alloy substrate, the COF dropped to 0.033, which is due to the layered structure of the MoS_2. Once the load was applied to the MoS_2 film, the nanosheets of the MoS_2 were distributed on the sliding track due to the layered structure and easy-to-shear ability of the MoS_2, which provided extra protection to the substrate. For the a-C:H film on the titanium alloy substrate, the COF dropped significantly to 0.056, which was also much better than the reference titanium alloy substrate and the MoS_2 film. Among all samples, superlubricity (COF~0.007) was achieved for the Mo-a film after 500 s of running-in. This superlubricity is triggered by the formation of the transfer film on the counter surface, which transitioned the initial high resistance steel-to-a-C:H contact to super low resistance steel-to-transfer film contact. Furthermore, the Mo-a film was tested at 5 N, 7 N, and 9 N loads to investigate the Mo-a film's friction coefficient and standard error tribological behavior, as shown in Figure 2b. The COF of Mo-a was still in the ultralow regimes of ~0.007, 0.008, and 0.007 at 5 N, 7 N, and 9 N, respectively. The primary reason behind this remarkable friction reduction to the ultralow regimes is due to the transition of disordered MoS_2 to ordered structures and the formation of incommensurate contact with a-C:H surfaces, as verified elsewhere [16,32].

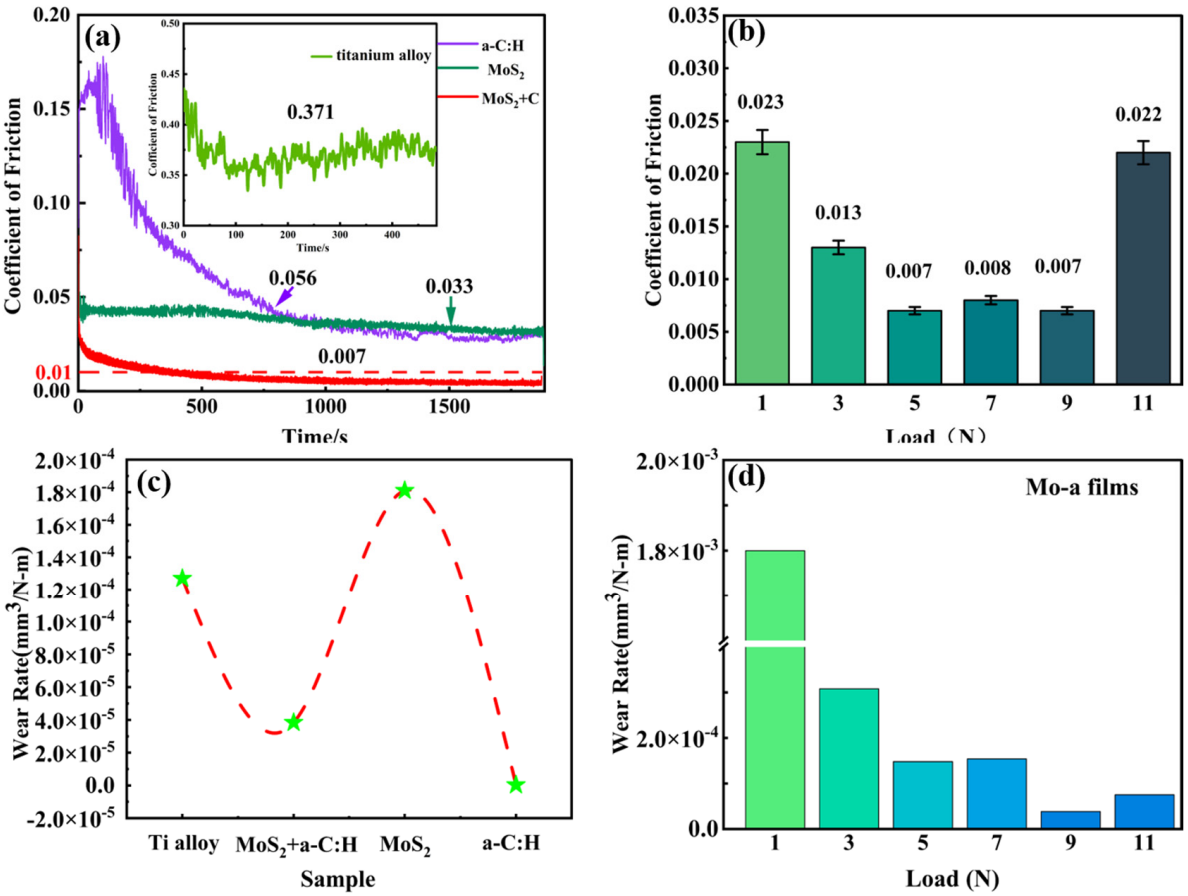

Figure 2. (**a**) Friction coefficient curves for the a−C:H film, MoS_2 film, Mo−a films, and titanium alloys under a 5 N load. (**b**) The average coefficient of friction and standard error of Mo−a films under different loads. (**c**) The rate of wear of different samples. (**d**) The wear rate of Mo−a films under different loads.

The anti-wear performance of the as-prepared films was investigated by calculating the wear rate, as shown in Figure 2c. It can be seen that the wear rate of the Mo-a composite film and a-C:H film was lower than that of the reference titanium alloy substrate. The wear rate of the titanium alloy substrate was 1.27×10^{-4} $mm^3/N^{-1} \cdot m^{-1}$, and the a-C:H film was 2.8×10^{-7} $mm^3/N^{-1} \cdot m^{-1}$, which means that the deposition of the a-C:H film reduced the wear rate by 1/453. Figure 2d shows the wear rate of the Mo-a composite film under different loads. The maximum wear rate of the composite film was 1.01×10^{-3} $mm^3/N^{-1} \cdot m^{-1}$ at a load of 1 N. The lowest wear rate of 3.84×10^{-5} $mm^3/N^{-1} \cdot m^{-1}$ was obtained at a load of 9 N.

3.3. Friction Reduction Mechanism Analysis

To fully understand the friction reduction mechanism, the relationship between the structural and chemical changes, and their role in the friction reduction at the sliding interface, Raman spectrometry was used. Figure 3 shows the Raman spectra of the wear scars and wear traces for the Mo-a films under different loads. Two characteristic peaks of MoS_2 around 390 and 410 cm^{-1} in the wear scars of different loads were $E^1{}_{2g}$ and A_{1g} [33]. These obvious peaks indicate that the MoS_2 component of the Mo-a films was successfully transferred to the counterpart balls. In the friction process, the MoS_2 transfer film on the counterpart balls gradually degraded as the load increased, as shown by the decreasing intensity of the characteristic peaks of MoS_2. As the experimental load exceeded 5 N, D and G peaks of the a-C:H film near 1370 and 1600 cm^{-1} appeared, which corresponded to the MoS_2 and carbon, which implies that the material that is transferred to the counter body in the form of a transfer film is composed of MoS_2 and carbon [34]. However, in the wear scars of the 1 N and 3 N loads, no D peak and G peak were detected, which implies that at low loads, the MoS_2 transfer film is not removed in large quantities, thus avoiding direct contact between the counterpart balls and the a-C:H film at the sliding interface. When the applied load exceeded 5 N, the D and G peaks detected in the wear scars completely differed from the Raman spectra of the a-C:H film, where the D peak of the wear scar appeared split, and the G peak shifted to a higher value. This splitting of the D peak and the shift in the G peak to a higher wave number indicates the graphitization of the a-C:H film [35]. This graphitization degree becomes more severe with the increase in load, implying that higher loads intensify the graphitization process. As mentioned in earlier studies, under high contact pressure, the main friction reduction mechanism in a-C:H films is the formation of graphite-like clusters of surface carbon layers at the sliding interface [36]. Research also shows that the high contact pressure leads to the decomposition of MoS_2 into Mo and S, which is favorable to carbon transformation and results in low friction [1].

Furthermore, the intensity variations in the D peak and G peak I_D/I_G also provide important information for the evolution of the carbon film structure. I_D/I_G values were obtained for 1, 3, 5, 7, 9, and 11 N loads using peak fitting, which were 0.58, 0.56, 0.59, 0.58, 0.59, and 0.50, respectively. From the values of the I_D/I_G of the wear tracks at different loads, it can be inferred that no significant structural evolution occurred in the a-C:H films.

As for the MoS_2 film, achieving single superlubricity with the MoS_2-flakes alone in a helium atmosphere is difficult. Furthermore, the I_D/I_G values of the a-C:H film at low loads of 1 N, 3 N, and 5 N were difficult to measure because the intensity of the D and G peaks in the Raman spectra was very weak. However, the I_D/I_G values in wear scar under 7 N, 9 N, and 11 N loads were 0.95, 0.93, and 0.9, respectively. The I_D/I_G ratio of the wear scars had a higher value at high loads than the value of I_D/I_G for wear traces, which indicates that the a-C:H film transferred to the ball is graphitized compared to the a-C:H film on the wear traces. The Raman spectra results of the wear scars are consistent with those of the previously published studies [37]. The I_D/I_G change can reflect the changes in the sp^3 content in the a-C:H films. An increase in the graphitization implies a decreased sp^3 carbon bond content [38].

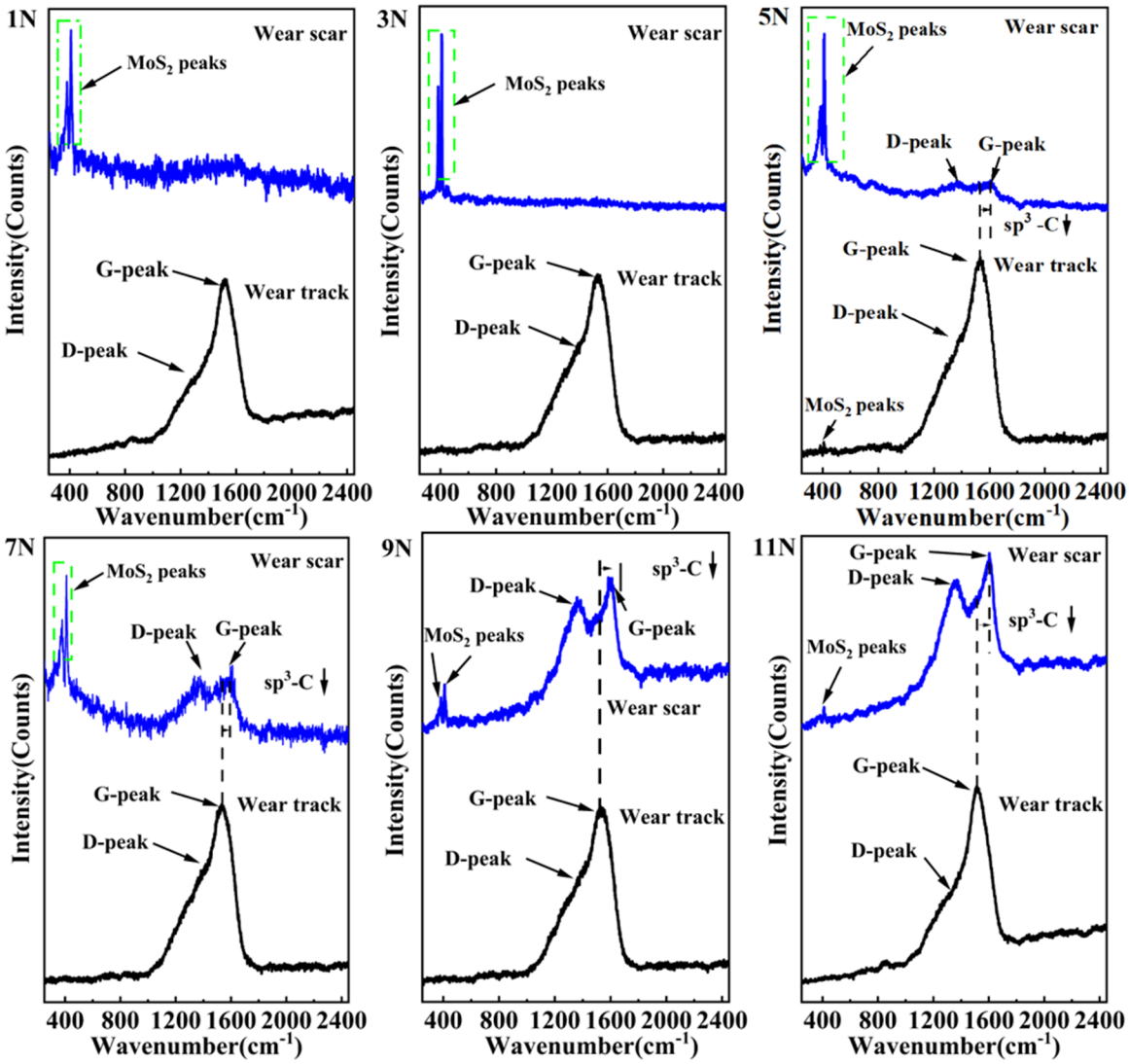

Figure 3. Raman spectrum of the wear scar and wear trace in the central region obtained at 1, 3, 5, 9, and 11 N loads.

Meanwhile, the blue shift of the G peak also indicates the transition of the sp^3 carbon structure to a graphite-like carbon structure during the friction process and reflects the increased graphitization process [39]. Meanwhile, the two weak characteristic peaks of MoS_2 were only detected on weak tracks with a 5 N load; however, no characteristic peaks were detected in other wear tracks. Thus, the effective friction reduction of the Mo-a film material system can be attributed to its conversion of the high-resistance steel and composite contact into super low resistance MoS_2 and a-C:H film contact.

Furthermore, the structural evolution of the wear debris of the Mo-a film was investigated with transmission electron microscopy (TEM). The TEM image of representative wear debris at the 5 N load is shown in Figure 4. Figure 4a shows the two main core areas of wear debris where the I region is enriched with highly ordered nanosheets of MoS_2 with an interlayer distance of 0.63 nm. In contrast, the II region is filled with curved graphene with an interlayer distance of 0.33 nm. In fact, during the sliding process, superlubricity can be triggered by many factors such as the applied load, the environment, shear stress, and the frictional chemistry of the contact area [40,41]. It has also been shown that the composite films of MoS_2 produced an ultra-low friction phenomenon, which was attributed to the fact that the sliding direction was related to the friction-induced direction parallel to the shear plane of the lamellar structure [42]. Previous studies have shown that frictional

stresses at the sliding interface cause structural transformations in the related materials of the friction pairs [1]. Thus, frictional stresses and tribochemical reactions accelerate the transformation of the amorphous carbon film into a graphene-like structure, which is consistent with the Raman characterization results of the wear scar in our work. Figure 4c shows the transformation of MoS_2 nanosheets into nanoscroll structures during stress-induced friction. The production of MoS_2 nanoscrolls significantly reduces the contact area in the contact zone. It demonstrates that contact stress is the main cause of the structural transformation of amorphous carbon films and MoS_2 nanosheets. Based on the above analysis, the superlubricity-achieving mechanism evolves in three broad stages as follows. (1) Amorphous carbon forms graphene under the action of frictional heat and contact stress, as demonstrated by previous studies [43]. At the same time, it has been shown that the formation of heterojunctions facilitates the reduction in contact areas and the elimination of strong carbon–carbon bonds across interfaces [44]. (2) The formation of MoS_2/graphene heterojunctions reduces the release of frictional energy. (3) The formation of nanoscroll structures reduces the contact area and suppresses energy dissipation.

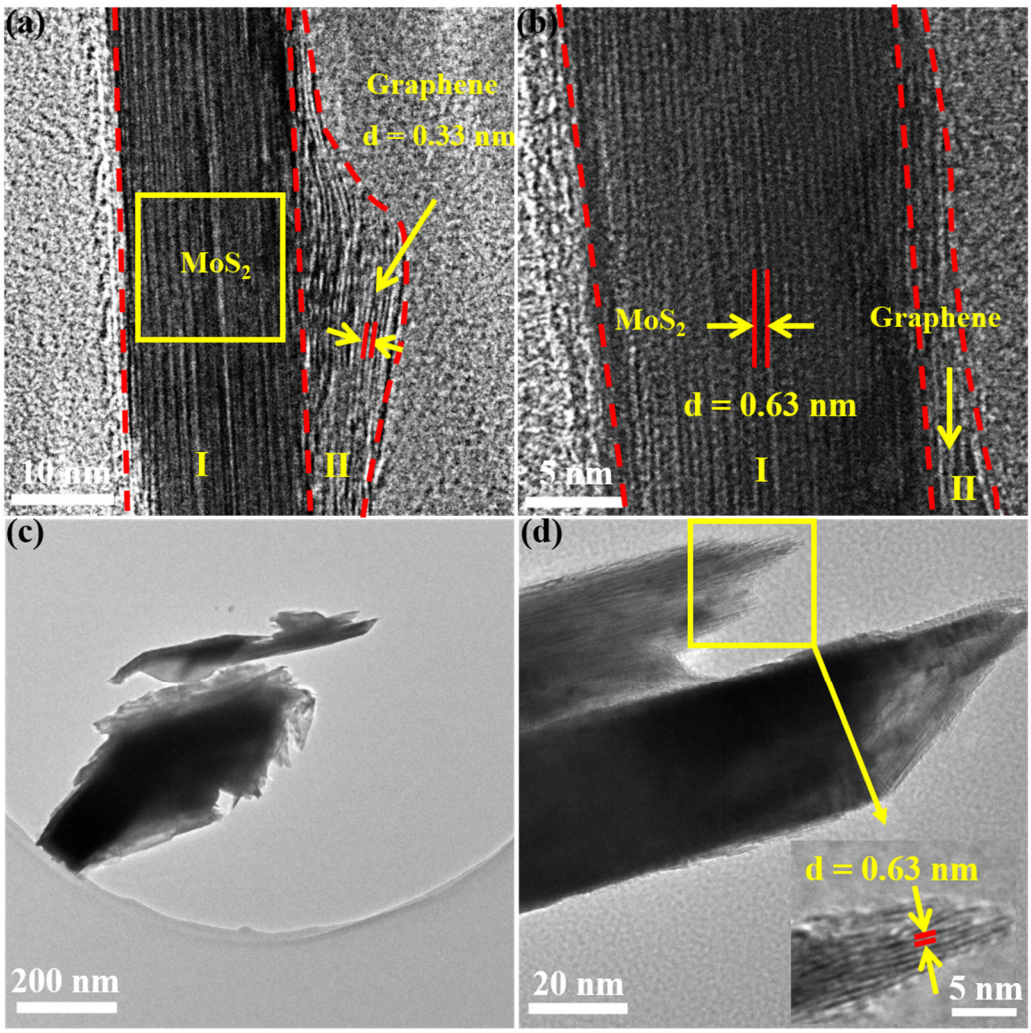

Figure 4. TEM image of the debris in the wear scar after the friction test under a 5 N load. (**a**,**b**) The wear debris consisted of layered MoS_2 and curved graphene, I is layered MoS_2, and II is curved graphene. (**c**,**d**) The wear debris consisted of MoS_2 nanotubes.

Figure 5 shows a schematic of the ultra-low friction mechanisms of the steel and Mo-a nanocomposites. When the composite films were subjected to a 5 N load, the coating material was removed and transferred to the surface of the counter body due to several phenomena such as the easy-to-shear ability of MoS_2, alteration of the a-C:H films into graphene-like lamellar structures, and the transformation of MoS_2 nanosheets into MoS_2 nanoscroll structures under high contact shear stress and frictional heat during the friction processes as verified with TEM and Raman characterization. Thus, this achievement of superlubricity can be attributed to the frictional heterojunction interface established by the graphene-like structure and the MoS_2 nanoscrolls, which provides incommensurate contact at the friction interface and remarkably reduces the friction to superlubric regimes.

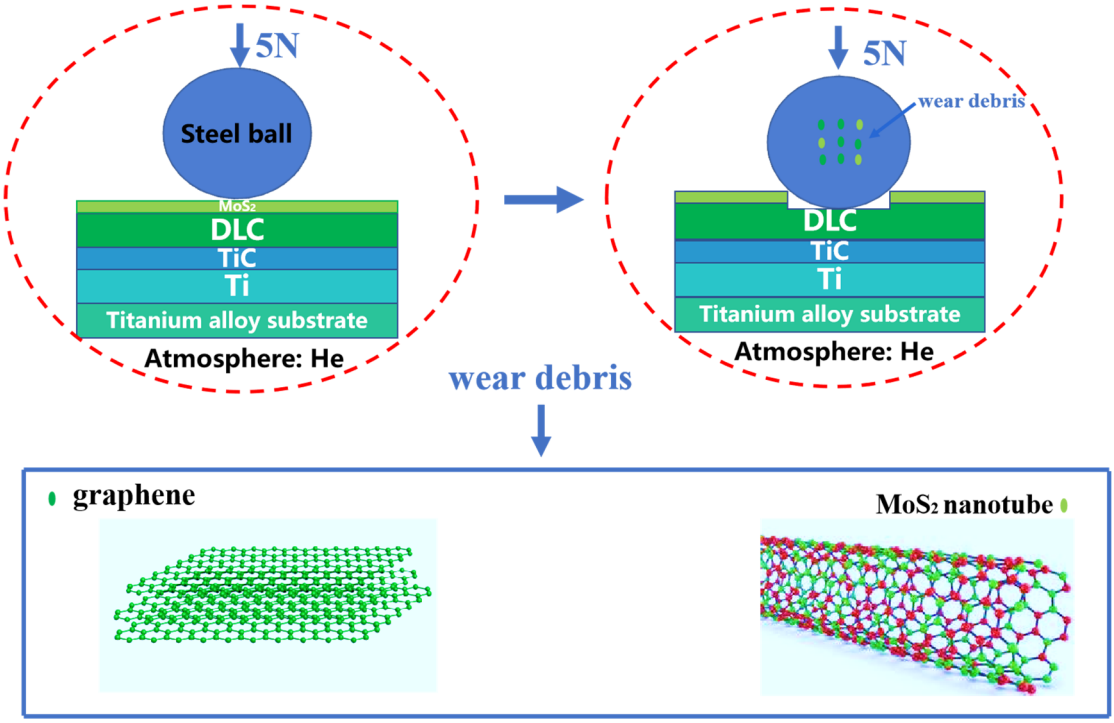

Figure 5. The ultra-low friction mechanism of steel-Mo-a films.

4. Conclusions

In this work, MoS_2, a-C:H, and Mo-a films were prepared on titanium alloy substrates by spraying and magnetron sputtering and investigated with reciprocating pin disk tribometer and high-resolution characterization techniques. The friction test results show that the Mo-a sample achieved superlubricity with a super low COF of ~0.007 on the titanium alloy substrates, which was remarkably lower than the a-C:H film (μ-0.056), MoS_2 film (μ-0.033), and titanium alloy (μ-0.371) in a He atmosphere. In addition, the fabrication of a-C:H film on the surface of the titanium alloy resulted in a reduction in the wear rate of three orders of magnitude compared to the titanium alloy substrates. It was verified by TEM that the MoS_2 and a-C:H films undergo structural evolution, with the MoS_2 nanosheets transforming into nanoscroll structures and the amorphous a-C:H transforming into layered graphene. The formation of highly ordered MoS_2 nanosheets and graphene heterojunctions resulted in an extremely low state of bond breakage and generation during friction. At the same time, the formation of the MoS_2 nanoscroll structure greatly reduced the frictional contact interface and synergy of the MoS_2 nanoscroll and graphene, which triggered favorable conditions for the achievement of the superlubricity and remarkable wear reduction rate for the Mo-a composite film.

Author Contributions: W.L.: Conceptualization, Investigation, Writing–original draft, Visualization; W.W.: Visualization, Investigation; M.C.: Visualization; Q.Z.: Visualization, Investigation; X.G.: Visualization, Investigation; K.R.: Visualization, Investigation; G.L.: Project administration, Funding acquisition; Z.G. (Zhongrong Geng): Project administration, Funding acquisition, Supervision; Z.G. (Zhenbin Gong): Project administration, Funding acquisition, Supervision. All authors have read and agreed to the published version of the manuscript.

Funding: The authors thank the National Natural Science Foundation of China (Grant No. NSFC-51527901), the Key Laboratory of Science and Technology on Wear and Protection of Materials, CAS (Grant No. CXJJ-21S047), and the National Natural Science Foundation of China (Grant No. NSFC-51865025). We also appreciate the Natural Science Foundation of Gansu Province of China (Grant Nos. 20JR5RA569 and N0.20JR5RA423).

Institutional Review Board Statement: Not applicable.

Informed Consent Statement: Not applicable.

Data Availability Statement: Not applicable.

Conflicts of Interest: The authors declare no conflict of interest.

References

1. Berman, D.; Erdemir, A.; Sumant, A.V. Approaches for Achieving Superlubricity in Two-Dimensional Materials. *ACS Nano* **2018**, *12*, 2122–2137. [CrossRef]
2. Zinatloo-Ajabshir, S.; Morassaei, M.S.; Amiri, O.; Salavati-Niasari, M. Green synthesis of dysprosium stannate nanoparticles using *Ficus carica* extract as photocatalyst for the degradation of organic pollutants under visible irradiation. *Ceram. Int.* **2020**, *46*, 6095–6107. [CrossRef]
3. Zinatloo-Ajabshir, S.; Shafaati, E.; Bahrami, A. Facile fabrication of efficient $Pr_2Ce_2O_7$ ceramic nanostructure for enhanced photocatalytic performances under solar light. *Ceram. Int.* **2022**, *48*, 24695–24705. [CrossRef]
4. Zinatloo-Ajabshir, S.; Salehi, Z.; Amiri, O.; Salavati-Niasari, M. Green synthesis, characterization and investigation of the electrochemical hydrogen storage properties of $Dy_2Ce_2O_7$ nanostructures with fig extract. *Int. J. Hydrog. Energy* **2019**, *44*, 20110–20120. [CrossRef]
5. Zinatloo-Ajabshir, S.; Salehi, Z.; Amiri, O.; Salavati-Niasari, M. Simple fabrication of $Pr_2Ce_2O_7$ nanostructures via a new and eco-friendly route; a potential electrochemical hydrogen storage material. *J. Alloys Compd.* **2019**, *791*, 792–799. [CrossRef]
6. Liu, S.; Shin, Y.C. Additive manufacturing of Ti_6Al_4V alloy: A review. *Mater. Des.* **2019**, *164*, 107552. [CrossRef]
7. Chen, K.; Zhou, Y.; Li, X.; Zhang, Q.; Wang, L.; Wang, S. Investigation on wear characteristics of a titanium alloy/steel tribo-pair. *Mater. Des.* **2015**, *65*, 65–73. [CrossRef]
8. Hu, T.; Hu, L.; Ding, Q. Effective solution for the tribological problems of Ti-6Al-4V: Combination of laser surface texturing and solid lubricant film. *Surf. Coat. Technol.* **2012**, *206*, 5060–5066. [CrossRef]
9. Karlsson, L.; Hultman, L.; Johansson, M.; Sundgren, J.-E.; Ljungcrantz, H. Growth, microstructure, and mechanical properties of arc evaporated TiCxN1−x ($0 \leq x \leq 1$) films. *Surf. Coat. Technol.* **2000**, *126*, 1–14. [CrossRef]
10. Oyama, S.T. (Ed.) *Introduction to the Chemistry of Transition Metal Carbides and Nitrides In The Chemistry of Transition Metal Carbides and Nitrides*; Springer: Dordrecht, The Netherlands, 1996; pp. 1–27.
11. Yang, Y.; Zhang, D.; Yan, W.; Zheng, Y. Microstructure and wear properties of TiCN/Ti coatings on titanium alloy by laser cladding. *Opt. Lasers Eng.* **2010**, *48*, 119–124. [CrossRef]
12. Selvam, P.T.; Pugazhenthi, R.; Dhanasekaran, C.; Chandrasekaran, M.; Sivaganesan, S. Experimental Investigation on the Frictional Wear Behaviour of TiAlN Coated Brake Pads. *Mater. Today Proc.* **2021**, *37*, 2419–2426. [CrossRef]
13. Erdemir, A.; Donnet, C. Tribology of diamond-like carbon films: Recent progress and future prospects. *J. Phys. D Appl. Phys.* **2006**, *39*, R311–R327. [CrossRef]
14. Liu, Y.; Erdemir, A.; Meletis, E. A study of the wear mechanism of diamond-like carbon films. *Surf. Coat. Technol.* **1996**, *82*, 48–56. [CrossRef]
15. Wang, S.; Wang, F.; Liao, Z.; Wang, Q.; Tyagi, R.; Liu, W. Tribological behaviour of titanium alloy modified by carbon–DLC composite film. *Surf. Eng.* **2015**, *31*, 934–941. [CrossRef]
16. He, D.; Zheng, S.; Pu, J.; Zhang, G.; Hu, L. Improving tribological properties of titanium alloys by combining laser surface texturing and diamond-like carbon film. *Tribol. Int.* **2015**, *82*, 20–27. [CrossRef]
17. Yu, X.; Du, R.; Li, B.; Zhang, Y.; Liu, H.; Qu, J.; An, X. Biomolecule-assisted self-assembly of CdS/MoS_2/graphene hollow spheres as high-efficiency photocatalysts for hydrogen evolution without noble metals. *Appl. Catal. B Environ.* **2016**, *182*, 504–512. [CrossRef]
18. Zhou, X.; Wang, Z.; Chen, W.; Ma, L.; Chen, D.; Lee, J.Y. Facile synthesis and electrochemical properties of two dimensional layered MoS_2/graphene composite for reversible lithium storage. *J. Power Sources* **2014**, *251*, 264–268. [CrossRef]

19. Jiang, J.-W.; Park, H.S. A Gaussian treatment for the friction issue of Lennard-Jones potential in layered materials: Application to friction between graphene, MoS_2, and black phosphorus. *J. Appl. Phys.* **2015**, *117*, 124304. [CrossRef]
20. Yu, G.; Zhang, Z.; Tian, P.; Gong, Z.; Zhang, J. Macro-scale super-low friction enabled when MoS_2 flakes lubricate hydrogenated diamond-like carbon film. *Ceram. Int.* **2021**, *47*, 10980–10989. [CrossRef]
21. Gong, Z.; Jia, X.; Ma, W.; Zhang, B.; Zhang, J. Hierarchical structure graphitic-like/MoS_2 film as superlubricity material. *Appl. Surf. Sci.* **2017**, *413*, 381–386. [CrossRef]
22. Berman, D.; Narayanan, B.; Cherukara, M.J.; Sankaranarayanan, S.K.R.S.; Erdemir, A.; Zinovev, A.; Sumant, A.V. Operando tribochemical formation of onion-like-carbon leads to macroscale superlubricity. *Nat. Commun.* **2018**, *9*, 1164. [CrossRef]
23. Mutyala, K.C.; Wu, Y.A.; Erdemir, A.; Sumant, A.V. Graphene—MoS_2 ensembles to reduce friction and wear in DLC-Steel contacts. *Carbon* **2019**, *146*, 524–527. [CrossRef]
24. Zhao, J.; Mao, J.; Li, Y.; He, Y.; Luo, J. Friction-induced nano-structural evolution of graphene as a lubrication additive. *Appl. Surf. Sci.* **2018**, *434*, 21–27. [CrossRef]
25. Scharf, T.W.; Goeke, R.S.; Kotula, P.G.; Prasad, S.V. Synthesis of Au–MoS_2 Nanocomposites: Thermal and Friction-Induced Changes to the Structure. *ACS Appl. Mater. Interfaces* **2013**, *5*, 11762–11767. [CrossRef] [PubMed]
26. Dong, B.; Guo, X.; Zhang, K.; Zhang, Y.; Li, Z.; Wang, W.; Cai, C. Combined effect of laser texturing and carburizing on the bonding strength of DLC coatings deposited on medical titanium alloy. *Surf. Coat. Technol.* **2022**, *429*, 127951. [CrossRef]
27. Grabarczyk, J.; Gaj, J.; Pazik, B.; Kaczorowski, W.; Januszewicz, B. Tribocorrosion behavior of Ti6Al4V alloy after thermo-chemical treatment and DLC deposition for biomedical applications. *Tribol. Int.* **2021**, *153*, 106560. [CrossRef]
28. Fu, Y.; Batchelor, A.W.; Wang, Y.; Khor, K. Fretting wear behaviors of thermal sprayed hydroxyapatite (HA) coating under unlubricated conditions. *Wear* **1998**, *217*, 132–139. [CrossRef]
29. Casiraghi, C.; Ferrari, A.C.; Robertson, J. Raman spectroscopy of hydrogenated amorphous carbons. *Phys. Rev. B* **2005**, *72*, 085401. [CrossRef]
30. Cui, W.; Lai, Q.; Zhang, L.; Wang, F. Quantitative measurements of sp3 content in DLC films with Raman spectroscopy. *Surf. Coat. Technol.* **2010**, *205*, 1995–1999. [CrossRef]
31. Li, H.; Zhang, Q.; Yap, C.C.R.; Tay, B.K.; Edwin, T.H.T.; Olivier, A.; Baillargeat, D. From Bulk to Monolayer MoS_2: Evolution of Raman Scattering. *Adv. Funct. Mater.* **2012**, *22*, 1385–1390. [CrossRef]
32. Cai, S.; Guo, P.; Liu, J.; Zhang, D.; Ke, P.; Wang, A.; Zhu, Y. Friction and Wear Mechanism of MoS_2/C Composite Coatings Under Atmospheric Environment. *Tribol. Lett.* **2017**, *65*, 79. [CrossRef]
33. Wang, Y.; Cong, C.; Qiu, C.; Yu, T. Raman Spectroscopy Study of Lattice Vibration and Crystallographic Orientation of Monolayer MoS_2under Uniaxial Strain. *Small* **2013**, *9*, 2857–2861. [CrossRef]
34. Habibi, A.; Khoie, S.M.; Mahboubi, F.; Urgen, M. Raman spectroscopy of thin DLC film deposited by plasma electrolysis process. *Surf. Coat. Technol.* **2017**, *309*, 945–950. [CrossRef]
35. Zeng, Q.; Eryilmaz, O.; Erdemir, A. Superlubricity of the DLC films-related friction system at elevated temperature. *RSC Adv.* **2015**, *5*, 93147–93154. [CrossRef]
36. Cloutier, M.; Harnagea, C.; Hale, P.; Seddiki, O.; Rosei, F.; Mantovani, D. Long-term stability of hydrogenated DLC coatings: Effects of aging on the structural, chemical and mechanical properties. *Diam. Relat. Mater.* **2014**, *48*, 65–72. [CrossRef]
37. Yu, G.; Qian, Q.; Li, D.; Zhang, Z.; Ren, K.; Gong, Z.; Zhang, J. The pivotal role of oxygen in establishing superlow friction by inducing the in situ formation of a robust MoS_2 transfer film. *J. Colloid Interface Sci.* **2021**, *594*, 824–835. [CrossRef] [PubMed]
38. Tamor, M.A.; Vassell, W.C. Raman "fingerprinting" of amorphous carbon films. *J. Appl. Phys.* **1994**, *76*, 3823–3830. [CrossRef]
39. Li, C.; Huang, L.; Yuan, J. Effect of sp3 Content on Adhesion and Tribological Properties of Non-Hydrogenated DLC Films. *Materials* **2020**, *13*, 1911. [CrossRef]
40. Hou, K.; Yang, S.; Liu, X.; Wang, J. The Self-Ordered Lamellar Texture of MoS_2 Transfer Film Formed in Complex Lubrication. *Adv. Mater. Interfaces* **2018**, *5*, 1701682. [CrossRef]
41. Cui, L.; Lu, Z.; Wang, L. Toward Low Friction in High Vacuum for Hydrogenated Diamondlike Carbon by Tailoring Sliding Interface. *ACS Appl. Mater. Interfaces* **2013**, *5*, 5889–5893. [CrossRef]
42. Donnet, C.; Martin, J.; Le Mogne, T.; Belin, M. Super-low friction of MoS_2 coatings in various environments. *Tribol. Int.* **1996**, *29*, 123–128. [CrossRef]
43. Gong, Z.; Shi, J.; Zhang, B.; Zhang, J. Graphene nano scrolls responding to superlow friction of amorphous carbon. *Carbon* **2017**, *116*, 310–317. [CrossRef]
44. Li, R.; Yang, X.; Zhao, J.; Yue, C.; Wang, Y.; Li, J.; Meyer, E.; Zhang, J.; Shi, Y. Operando Formation of Van der Waals Heterostructures for Achieving Macroscale Superlubricity on Engineering Rough and Worn Surfaces. *Adv. Funct. Mater.* **2022**, *32*, 2111365. [CrossRef]